Exploring the Possible Role of Small-Scale Terrain Drag on Stable Boundary Layers over Land

G. J. STEENEVELD AND A. A. M. HOLTSLAG

Wageningen University, Wageningen, Netherlands

C. J. NAPPO

NOAA/Air Resources Laboratory, and NOAA/Atmospheric Turbulence and Diffusion Laboratory, Oak Ridge, Tennessee

B. J. H. VAN DE WIEL

Wageningen University, Wageningen, Netherlands

L. MAHRT

College of Oceanic and Atmospheric Sciences, Oregon State University, Corvallis, Oregon

(Manuscript received 26 June 2007, in final form 25 February 2008)

ABSTRACT

This paper addresses the possible role of unresolved terrain drag, relative to the turbulent drag on the development of the stable atmospheric boundary layer over land. Adding a first-order estimate for terrain drag to the turbulent drag appears to provide drag that is similar to the enhanced turbulent drag obtained with the so-called long-tail mixing functions. These functions are currently used in many operational models for weather and climate, although they lack a clear physical basis. Consequently, a simple and practical quasi-empirical parameterization of terrain drag divergence for use in large-scale models is proposed and is tested in a column mode. As an outcome, the cross-isobaric mass flow (a measure for cyclone filling) with the new scheme, using realistic turbulent drag, appears to be equal to what is found with the unphysical long-tail scheme. At the same time, the new scheme produces a much more realistic less-deep boundary layer than is obtained by using the long-tail mixing function.

1. Introduction

After sunset under clear skies, the land surface cools rapidly, the potential temperature increases with height, and a stable boundary layer (SBL) develops. Generally, the dominant physical processes in the SBL are turbulent mixing, radiative cooling, and the interaction of the atmosphere with the land surface (e.g., Beljaars and Holtslag 1991; André and Mahrt 1982). Also, small-scale features such as gravity waves, katabatic flows, drainage flows, and effects of land surface heterogeneity can influence the SBL structure. The large variety of SBL physical processes, their nonlinearity, and their interactions hampers our ability to understand and to model the SBL on a large spatial scale (e.g., in operational forecast models; Cuxart et al. 2006; Holtslag 2006).

Despite the problems mentioned above, Steeneveld et al. (2006a) showed that the SBL can be satisfactorily modeled *on a local scale* for a broad stability range (i.e., on a specific site and for clear, calm, and windy or cloudy nights). This can be achieved when the forcings (geostrophic wind speed and advection) and the local characteristics of the soil and vegetation are well known. Also, the physical processes of turbulent mixing, radiation divergence, and soil heat flux should be accounted for in detail. Steeneveld et al. (2006a) use a turbulent mixing scheme that agrees with tower observations and large eddy simulation results, and shows nearly vanishing turbulent mixing for large Richardson numbers (Ri) (e.g., Beljaars and Holtslag 1991; Duynkerke 1991, hereinafter D91). We will refer to this scheme as a "short tail" scheme.

Contrary to this local approach, many large-scale

Corresponding author address: Gert-Jan Steeneveld, P.O. Box 47, 6700 AA Wageningen, Netherlands.
E-mail: gert-jan.steeneveld@wur.nl

DOI: 10.1175/2008JAMC1816.1

models with a short-tail formulation suffer from insufficient cyclone filling (i.e., low pressure systems are forecast to be too deep and their lifetime is longer than observed; Beljaars and Viterbo 1998; Viterbo et al. 1999; Nielsen and Sass 2005; Holtslag 2006). Therefore, large-scale models require more drag than is provided by the short-tail formulation. This is currently achieved by applying "enhanced turbulent mixing" or a nonphysical "long tail" formulation, with nonzero turbulent mixing and drag for large Ri. An additional argument in favor of the long-tail formulation is that it also prevents models from unrealistic runaway surface cooling. Since there is no physical justification for the enhanced mixing approach, the current mixing formulations for both the surface layer and the SBL are strongly based on model performance and not on physical reality (Louis 1979; Beljaars and Viterbo 1998; Zilitinkevich et al. 2002).

Although the enhanced mixing approach provides satisfying synoptic flow, a key drawback of this approach is the poor representation of some critical aspects of the SBL. First, the SBL becomes typically a factor of 2–3 too deep, and the mean stratification is underestimated (Ek et al. 2003; Cuxart et al. 2006). This has clearly negative consequences for forecasting the dispersion of pollutants. Second, the typical nocturnal wind maximum or low-level jet (LLJ) is forecast to be at a too-high altitude and is too weak (e.g., Steeneveld et al. 2008). This gives erroneous horizontal transport of, for example, humidity from the Gulf of Mexico to the Midwest (Cheinet et al. 2005). Also, the backing of the wind is insufficient in stable stratification, not only over land, but also over sea (Brown et al. 2005). This mismatch of the SBL structure has substantial impact on the ability to forecast fog, air quality, and frost. Obviously, the present long-tail parameterization is unsatisfactory from a physical point of view and improvement is needed.

The long-tail formulation is often justified by means of mesoscale circulations because of land surface heterogeneities smaller than the model grid cell. Asymmetric cooling on the subgrid scale can generate additional terms in the flux calculations due to spatial averaging of the nonlinear flux–gradient relationship (Mahrt 1987). However, McCabe and Brown (2006) show that this effect cannot fully account for the requested additional mixing for their model and study area, but only contributes to the additional drag near the surface (first 10 m).

Hence, there is a clear need to examine other possible mechanisms that can account for the apparently needed drag. Therefore, we have to realize that drag is not necessarily only turbulent drag (with strong mixing), but can also be due to processes with less strong mixing properties. McCabe and Brown (2006) speculate that gravity wave drag or other forms of terrain drag might be a possible candidate. This is supported by earlier studies in, for example, Chimonas and Nappo (1989).

We emphasize that it is currently unclear what amount of the applied enhanced drag in the SBL is really justifiable to the SBL, or whether it is used to compensate for errors somewhere else in the models. Other processes than turbulence, and also daytime physical processes, might contribute to the drag, although their individual role has not been understood and quantified yet. Because the role of the SBL on cyclone development in NWP models is under debate, we assume as a working hypothesis that the cyclone development is influenced by SBL drag and that gravity wave drag can contribute to this.

We analyze the possible impact of gravity wave–induced terrain drag. We also propose a *practical, quasi-empirical* method to account for terrain drag on the SBL, and we will show that this method provides both a realistic SBL height and LLJ. On the other hand, the parameterization also provides sufficient cyclone filling *at the same time*. The paper is organized as follows: section 2 gives some background material and section 3 presents a brief theoretical background. In section 4 a simple parameterization for wave stress in the SBL is proposed. The discussion and conclusions follow in sections 5 and 6, respectively.

2. Background

There are few areas greater than 2 or 3 km^2 of the earth's surface that are flat. Spatial variance of terrain height exists on all scales of atmospheric motions ranging from mountains and valleys on the global scale to hillocks and gullies on the SBL scale. On the global scale, the diurnal cycle has little influence on the atmospheric drags produced by the large-scale terrain features. However, daytime convection tends to overwhelm the perturbations of the boundary layer flow by small-scale terrain irregularities, but in the SBL these perturbations can be important. Examples of these types of perturbations include form drag, flow blocking, channeling, rotors, hydraulic jumps, vortex shedding, turbulent wakes, and buoyancy waves. These stresses are not considered in similarity theory, and their effects are not simulated in the treatments of the SBL in mesoscale models.

The integrated effects of terrain-height variance during convective conditions have been approached by the use of an "effective" surface roughness parameter (e.g., Wood and Mason 1993). However, such a parameter

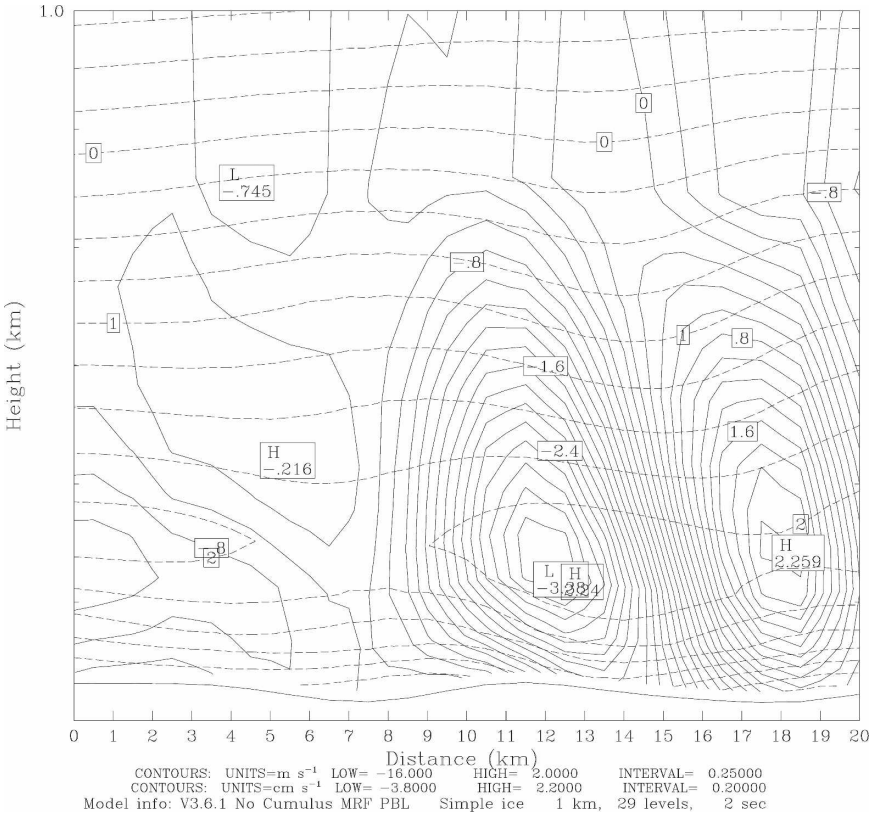

FIG. 1. North–south cross section of modeled (MM5; 1 km × 1 km horizontal resolution) boundary layer flow over a small surface corrugation with an amplitude of about 7.5 m and a wavelength of about 8 km for a calm night in the CASES-99 experimental campaign [1200 UTC (0600 LT) 23–24 Oct 1999]. Solid lines: vertical wind speed (cm s^{-1}); dashed line: wind component perpendicular to the orography (m s^{-1}).

appears not to be accurate under stable conditions when gravity waves are excited. One reason for this is that the effective surface roughness is independent of the atmospheric flow and thermal stratification, as is the case with the aerodynamic surface roughness, z_0.

In this study we explore the role of small-scale [amplitude O(10 m) and horizontal scale O(1–10 km)] orographically generated wave stress and whether parameterization of its flux divergence in the SBL impacts the flow. Wave stress divergence in the SBL may reduce the mean flow (analogous to waves generated by large mountains) without the need for intensive turbulent mixing. Despite its potential impact, large-scale models currently do not specifically account for wave stress in the SBL.

As an example, Fig. 1 shows a 20-km north–south cross section of modeled horizontal and vertical wind speed by the fifth-generation Pennsylvania State University–National Center for Atmospheric Research Mesoscale Model (MM5) at the end of a relatively calm night (geostrophic wind 6 m s^{-1}) during the 1999 Cooperative Atmosphere–Surface Exchange Study (CASES-99) field campaign (Steeneveld et al. 2008). Although the CASES-99 terrain is often referred to as relatively flat and homogeneous (Poulos et al. 2002), the U.S. Geological Survey (USGS) land surface database (used for the land surface properties in MM5) indicates that the terrain is gently undulating with a wavelength of about 8 km and an amplitude of about 7.5 m (see also Fig. 3 below).

Figure 1 shows that the flow is seriously "influenced" by the orography and that the model produces standing waves that extend up to 350 m above the main terrain height, and the wave crests tilt upstream (Nappo 2002). Thus, even for this relatively simple orography, complex flow structures are present that are resolved in high-resolution models, but not in large-scale models. Unfortunately, observing these structures in the field is also complicated. Tower measurements at a single station cannot reveal this 2D structure, and obtaining an adequate sample size perpendicular to the wave phase lines with an aircraft might be a serious problem.

Therefore, we have to rely on model results to get an indication of the flow field. Note that the flow in Fig. 1 is formally not exactly a linear flow since turbulent friction is incorporated in this simulation, and the wind speed and stratification are not constant with height.

Large-scale models deal with three effects to account for the impact of (mountain) orography on the flow (Lott and Miller 1997):

1) turbulent form drag due to pressure forces,
2) gravity wave drag, and
3) flow blocking.

Turbulent form drag is often parameterized using an effective roughness length approach: the roughness length for momentum is increased if the amplitude of the underlying orography is sufficiently large, and the roughness length for scalars is decreased. An alternative approach is an explicit prescription of the turbulent flux enhancement with height (Brown and Wood 2001; Rontu 2006). Brown and Wood (2003) showed that the effective roughness length approach works satisfactorily (at least for large winds) in the SBL only in the case where gravity waves are absent, and therefore we will not consider this subject in more detail.

Mountains or ridges can generate stationary gravity waves in a stably stratified medium. The role of propagating gravity waves in the ABL dynamics is actively discussed (e.g., Finnigan 1999; Brown et al. 2003). Although specific knowledge of waves in the SBL is limited, there is sufficient observational (e.g., Kurzeja et al. 1991; Nappo 1991; Sun et al. 2003; Cheng et al. 2005) and theoretical (Chimonas and Nappo 1989; Nappo and Chimonas 1992; Belcher and Wood 1996) evidence to suggest that gravity waves are important. Since waves generate Reynolds stresses, they might play an important role on the dynamical evolution of the SBL (Einaudi and Finnigan 1981; Finnigan 1999).

Orographically generated waves propagate upward and the associated wave stress is in principle constant with height (provided constant wind speed and stratification), unless wave dissipation occurs (Eliassen and Palm 1960). However, wave dissipation can occur in regions of wave saturation (Fritts 1984) where background winds and stratification change rapidly with height as in the SBL. Also, when gravity waves are excited, the wave field can become convectively unstable at a certain level (i.e., overturning) and the waves will break. This will certainly happen when the waves approach a critical level (i.e., where wind speed $U = 0$). Consequently, a divergence of the wave stress can occur, and this will decelerate the flow. This mechanism is well understood for large mountain ridges. However, the SBL is shallow, and one can expect that small-scale orography can also significantly influence the SBL flow through gravity wave propagation. Nappo (2002) and Chimonas and Nappo (1989) indeed theoretically showed that the magnitude of the SBL wave stress and turbulent stress are of the same order during weak winds.

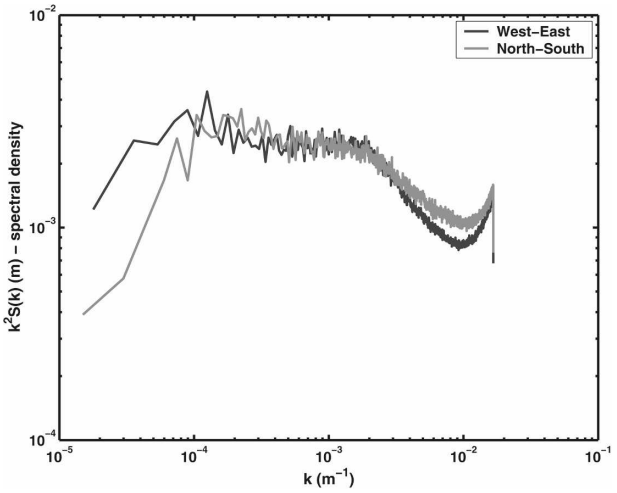

FIG. 2. Spectrum of the orography in an area of 40 km × 40 km around the CASES-99 central site. The vertical dashed line indicates the cutoff wavenumber above which large-scale models neglect the effect of orographic wave stress.

Large-scale models account for mountain gravity waves resulting in forecast quality improvement (Palmer et al. 1986). However, normally *only orography on horizontal scales larger than 5 km* (Beljaars et al. 2004) is considered. This may be correct for typical free-tropospheric stratification, but is not a priori correct for the SBL, where smaller horizontal scales may impact gravity wave generation.

Figure 2 shows the mean spectral densities of the orography, calculated from the 0.33″ USGS database (available online at http://seamless.usgs.gov/) for about 40 km × 40 km around the CASES-99 central mast. For small scales the spectrum is subject to aliasing. We find that the variability in the orography (both in x and y direction) is the same over a broad range of scales, but, more important, they are almost level between $k = 2 \times 10^{-4}$ and 2×10^{-3} m^{-1}. So the clear cutoff of $k = 2 \times 10^{-4}$ m^{-1} for the contributing scales to wave drag in large-scale models is not a priori justified (at least for the current area).

Finally, flow blocking occurs when the vertical Froude number $\mathrm{Fr} = U/(NH) < 1$, where U is the wind speed, N is the Brunt–Väisälä frequency, and H is the orography amplitude. In that case, the stratification is so strong that the flow is unable to pass over the topography, and over a certain depth the flow becomes

blocked. Hence, a force is directed from the orography to the air. Large-scale models account for flow blocking for the large scales (e.g., Lott and Miller 1997). For moderate orography it is well known that flow blocking may be important (Grant 1994; Holden et al. 2000), but it is not accounted for in large-scale models. Flow blocking might be relevant for SBL modeling as well, but for simplicity it will not be treated here.

In the next section, we examine the wave contribution to the total drag in stable conditions and compare this drag with the required drag in large-scale models.

3. Theory

Large-scale models often utilize an eddy diffusivity K_m to calculate the turbulent mixing in the SBL (e.g., D91; Holtslag 1998):

$$K_m = (\kappa z)^2 \left| \frac{\partial \mathbf{U}}{\partial z} \right| F_m(\mathrm{Ri}), \tag{1}$$

where κ is the von Kármán constant (taken as 0.4 here), z is the height above the ground, $\mathbf{U}$ is the modulus of the wind speed, and Ri is the gradient Richardson number.

The stability function for momentum, F_m, limits K_m for stronger stratification, and its form has been determined from many turbulent field observations (via the so-called flux–profile relationships), in particular for the surface layer (e.g., McVehil 1964; Oke 1970; Businger et al. 1971; Skibin and Businger 1985; Beljaars and Holtslag 1991; Howell and Sun 1999; Steeneveld et al. 2006a; Baas et al. 2006) and from large-eddy simulations (LES) (e.g., Beare et al. 2006). D91 proposes $F_m = \varphi_m^{-2}$, with

$$\varphi_m = 1 + \beta \frac{z}{\Lambda} \left(1 + \frac{\beta}{\alpha} \frac{z}{\Lambda} \right)^{\alpha - 1}. \tag{2}$$

Herein Λ is the local Obukhov length. This functional form has been well validated by field observations in Cabauw (D91) and CASES-99 (Steeneveld et al. 2006a). Here we take $\alpha = 0.9$ and $\beta = 5$ to mimic a short-tail formulation.

To estimate the wave drag (τ_{wave}), one may use linear theory (see support in Fig. 3 below). Then the wave drag for an idealized sinusoidal surface corrugation for constant wind speed and stratification is given by (Belcher and Wood 1996; Nappo 2002)

$$\tau_{\mathrm{wave}} = \begin{cases} \frac{1}{2}\rho_0 k_s (UH)^2 \sqrt{\frac{N^2}{U^2} - k_s^2} & \text{for} \quad \frac{N}{U} > k_s \\ 0 & \text{for} \quad \frac{N}{U} \le k_s. \end{cases} \tag{3}$$

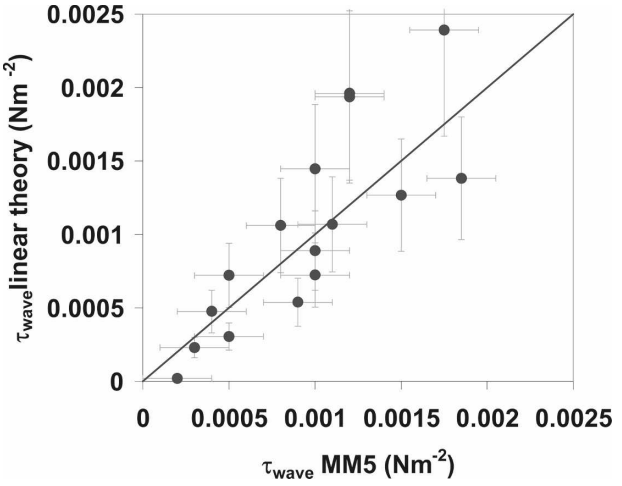

FIG. 3. Modeled near-surface wave drag [linear theory; Eq. (3)] vs resolved wave drag from the high-resolution MM5 for the night of 23–24 Oct 1999 during the CASES-99 experiment.

Here, k_s is the wavenumber, ρ_0 is the air density, and U is the background wind speed perpendicular to the orography. Equation (3) reduces for weak winds to (Nappo 2002)

$$\tau_{\mathrm{wave}} = \frac{1}{2}\rho_0 k H^2 N U. \tag{4}$$

Note that this result can also be deduced from dimensional analysis realizing that N and U are the relevant atmospheric variables and k_s and H are the relevant terrain parameters.

4. Model impact of small-scale terrain drag

a. Wave drag from MM5

High-resolution models such as MM5 are able to resolve the wave perturbations that are generated by the underlying orography. To quantify the resolved wave drag from forecasted MM5 fields, the u and w components along a transect were linearly detrended and the mean was subtracted. Then τ_{wave} was calculated as the covariance of the remaining perturbations along the transect. This was done for many levels close to the ground. To examine the plausibility of the linear theory, we compare the wave drag obtained from Eq. (3) (using mean profiles from MM5 as input) with the resolved wave drag in MM5. The H and N are obtained from Fig. 1 in which the highest altitude is 432 m (MSL) and the lowest is 415 m, which gives $H = 7.5$ m. Figure 1 also reveals a wavelength of 8000 m; thus $k_s = 2\pi/8000\ \mathrm{m}^{-1}$, and we take the density $\rho = 1\ \mathrm{kg\ m}^{-3}$ constant for simplicity. Note that using Eq. (4) instead of Eq. (3) provided approximately similar results.

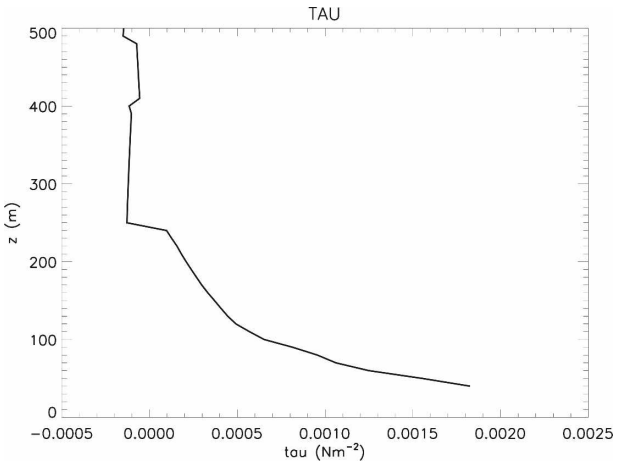

FIG. 4. Vertical profile of resolved orographic wave drag in the MM5 simulation for the night of1200 UTC (0600 LT) 23–24 Oct 1999 in CASES-99 (see also Fig. 1).

Figure 3 compares the resolved near-surface wave drag from the high-resolution MM5 run with the wave drag from linear theory for the night of 23–24 October 1999 (same night as in Fig. 1). The two methods provide the corresponding quantity of wave drag, although some scatter is present. Error bars in the graph indicate the tolerance of the wave drag, and these were obtained from standard error propagation calculations. The result shows that the linear theory is a proper tool to provide a rough estimate for the orographic wave drag in the SBL.

Next, we investigate the decay of the wave drag with height. Wave stress decay will provide a net force on the air layer over which it decays, which will trigger a flow deceleration. Figure 4 clearly shows that in the MM5 simulation, substantial wave drag decay occurs over the SBL, and the decay is stronger close to the ground than aloft. This decay implies that orographic wave drag influences the SBL dynamics. Both results from MM5 will be used to design a simple parameterization.

For completeness, MM5 was run in a 1600 m × 1600 m area with for four nested grids, with the inner nest at a 1-km horizontal resolution. Furthermore, the European Centre for Medium-Range Weather Forecasts (ECMWF) provided the initial and boundary conditions every 6 h. We used the Medium-Range Forecast (MRF) boundary layer scheme and the cloud radiation scheme. Further details on those simulations can be found in Steeneveld et al. (2008).

b. Column model: Dynamics

Small-scale wave drag due to orography should be parameterized in large-scale models, since it is a subgrid process. Then, the prognostic equations for wind speed become

$$\frac{\partial U}{\partial t} = f(V - V_g) - \frac{\partial \overline{u'w'}}{\partial z} + \frac{1}{\rho}\frac{\partial \tau_{\text{wave},u}}{\partial z} \quad \text{and} \tag{5}$$

$$\frac{\partial V}{\partial t} = -f(U - U_g) - \frac{\partial \overline{v'w'}}{\partial z} + \frac{1}{\rho}\frac{\partial \tau_{\text{wave},v}}{\partial z}, \tag{6}$$

with U_g and V_g as the x and y components of the geostrophic wind, f as the Coriolis parameter, the second term on the RHS as the turbulent flux divergence, and the third term as the divergence of the terrain stress.

To account for the divergence of the wave drag, we follow the result of Fig. 3. We assume that the terrain stress is at maximum at the surface, and that it decreases quadratically with height up to the scale depth of the SBL where it vanishes:

$$\tau_{\text{wave}}(z) = \tau_{\text{wave}}(0)(1 - z/h)^2, \tag{7}$$

with h as the SBL height, defined as the height where the local u_* is 5% of its surface value and divided by 0.95 (Cuxart et al. 2006). We calculate $\tau_{\text{wave}}(0)$ in Eq. (7) with Eq. (4), and N and U are obtained from the lowest half of the SBL. Using Eq. (3) instead of Eq. (4) provided approximately similar results here also.

We mention that a linear instead of a quadratic stress decay with height would lead to similar model results (not shown). In addition, an arbitrarily chosen 10% of the terrain stress divergence is allowed to extend above the SBL. However, we found that altering the 10% criterion in the range between 1% and 5% does not modify the results significantly. Note that our proposal relies on the correct formulation of the boundary layer height, which is not a priori clear for the SBL (e.g., Vickers and Mahrt 2004; Steeneveld et al. 2007).

Despite the support from MM5 for the quadratic shape in Eq. (7), in certain atmospheric conditions, the functional form of the wave stress dissipation might be different from quadratic, and this height dependence does not necessarily scale with the SBL height. However, no other clearly definable height scale for this divergence is currently available. Therefore, as a working hypothesis, we use the SBL height for the vertical scale in Eq. (7).

Additional support for the divergence of the wave stress in the SBL is given in Brown et al. (2003), who reason that orographically generated gravity waves propagate upward but cannot pass the boundary layer top. Since the nocturnal SBL develops against the background of a near-neutral residual layer, waves cannot propagate (totally) into the free atmosphere (Zilitinkevich 2002). Also, Grisogono (1994) and Jiang et al. (2006) found that in nonideal conditions when tur-

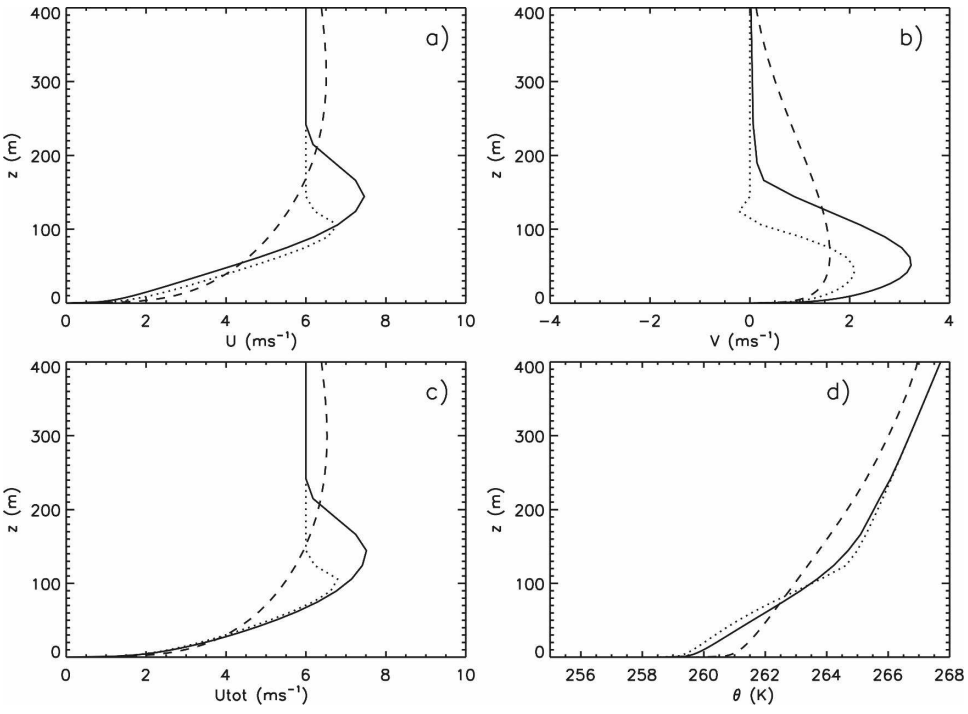

FIG. 5. Modeled wind speed and potential temperature profiles after 8-h simulation with a short-tail formulation (dotted line), the LTGr formulation (dashed line), and the new scheme with short tail + wave drag (solid line): (a) U, (b) V, (c) U_{total}, and (d) θ.

bulence is acting on the wave perturbations, the wave stress can be absorbed by the boundary layer. Consequently, a major part of the wave stress generated near the surface can be supported by momentum loss from the SBL and represented in the governing equations for the dynamics (Nappo 2002).

In addition to the physical aspects, numerical aspects are important for a parameterization. The introduction of wind tendencies due to breaking waves on a single grid level (e.g., due to a critical level) might result in numerical problems, which should be avoided. Since we utilize the SBL height, and a layer-averaged mean wind and stratification for our parameterization, it is robust, and not dependent on state variables at a single model level.

Finally, the quadratic wave drag dissipation does not circumvent the lack of mixing aloft in NWP or GCM models. For example, the breakdown of wave drag due to shear at the jet stream results in mixing. Unfortunately, coarse model resolution nearly prohibits reaching the $\text{Ri} < \text{Ri}_{\text{crit}}$. The same holds for resolved mountain waves in the upper troposphere.

c. Column model: Case study

To examine the behavior of the parameterization, we utilize a 1D vertical model for the boundary layer (D91) that represents a short-tailed formulation for the calculation of the turbulent fluxes. We start with a boundary layer with initial mean state of $\theta = 265$ K for $0 < z < 100$ m and 0.01 K m^{-1} increasing above $z > 100$ m, and the atmosphere is considered to be dry. The surface has a $z_0 = z_{0\text{h}} = 0.1$ m and we assume $H = 10$ m and $L_x = 1000$ m (with the corrugations parallel with y axis) for illustrating the effect of accounting for terrain stress. The model integration is for 68 h and for the current study we apply a 40-layer logarithmically spaced grid. This provides fine resolution near the surface ($\Delta z = 0.7$ m) and coarser near the model top (800 m). The geostrophic wind is $U_g = 6$ m s^{-1} and $V_g = 0$ m s^{-1} and $f = 1.39 \times 10^{-4}$ s^{-1} (equivalent to 73°N). At the surface, we solve the energy budget to predict the surface temperature. Hence, the surface turbulent heat flux is interdependent on the surface temperature and the ground heat flux (as in reality; Steeneveld et al. 2006b). The graybody emissivity scheme of Garratt and Brost (1981) is utilized to account for radiative flux divergence.

The modeled wind speed and potential temperature profiles after 8 h are shown in Fig. 5. We show results of three simulations: one using the D91 formulation [Eq. (2)], one using the long-tailed Louis–Tiedtke–Geleyn (LTG)-revised (LTGr; Beljaars and Viterbo 1998) for-

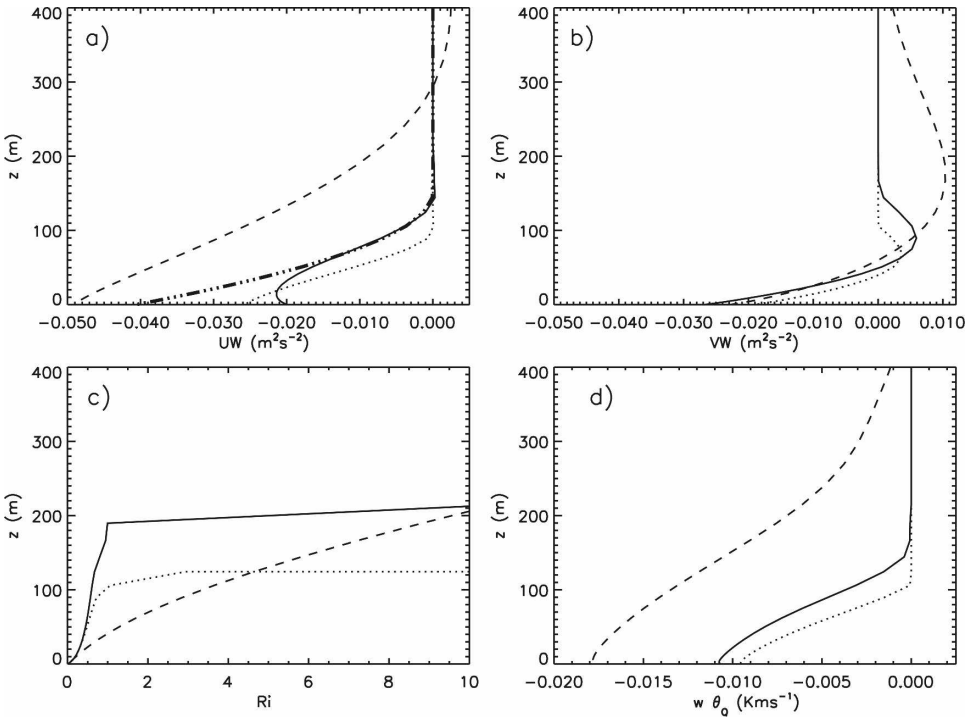

FIG. 6. Modeled profiles of turbulent momentum fluxes (a) $\overline{uw}$, (b) $\overline{vw}$, and (c) gradient Richardson number, and (d) turbulent sensible heat flux ($\overline{w\theta}$) after 8-h simulation for short-tail formulation (dotted line), the LTGr formulation (dashed line), and the new scheme with short tail + wave drag (solid line). In (a), the thick dotted–dashed line is the forecast wave stress profile.

mulation, and one using D91 plus terrain stress [Eq. (7)] included. After 10 h the model reaches a stationary state (not shown). We find some characteristic differences between the model formulations. Relative to the original D91 formulation, the LLJ is stronger with the new scheme and is located at higher altitude (90 m with D91 and 140 m with the new scheme). The v component of the wind is larger with the new scheme over a 200-m-deep layer, with the strongest impact at 50-m height where the maximum speed changed from 2.1 to 3.8 m s^{-1}, and the modulus of the LLJ speed changed from 6.5 to 7.5 m s^{-1}. Note that h is deeper than with the D91 formulation, although this seems to contradict the extra removal of momentum from the mean flow. However, the current formulation removes most of the momentum near the surface, which means the shear over the total SBL increases and thus also the shear production, the turbulent mixing, and consequently the SBL depth. The LLJ accelerates much slower in the new scheme compared with the D91 scheme, and we find an inflection point in the wind profile at $t = 4$ h (not shown). This will provide in reality a dynamically unstable profile.

More important is the comparison between the new scheme and the LTGr scheme results. The new scheme gives an LLJ of 7.5 m s^{-1} at 150 m, where the LTG scheme lacks a clear LLJ. As such, the new scheme provides a much smaller and more realistic boundary layer depth than the LTGr. The wind speed gradient within the SBL is larger with the new scheme than with LTGr, and also the wind turning with height is much smaller with LTGr than with the new scheme. The thermal structure reveals a stronger stratification with terrain stress included at $t = 4$ h (not shown) and a more mixed structure after 8 h. Furthermore, the thermal structure of the LTGr is less stable over a deep layer than for the other simulations.

Figure 6 depicts the modeled turbulent momentum fluxes (together with the modeled height-dependent terrain stress), the turbulent heat flux, and Ri. After $t = 4$ h the terrain stress is the main contributor to the total stress, and substantial to account for in large-scale models. The turbulent stress is smaller with the new formulation than with the D91 formulation, although this counteracts the increase of surface friction that we want to achieve. Note that the turbulent heat flux is hardly affected. The Ri number increases strongly with height and shows a sudden increase at 110 m for a run with Eq. (3) and at 200 m for the case with terrain stress included. The long-tailed LTGr formulation provides a more gradual increase of Ri with height. The height-

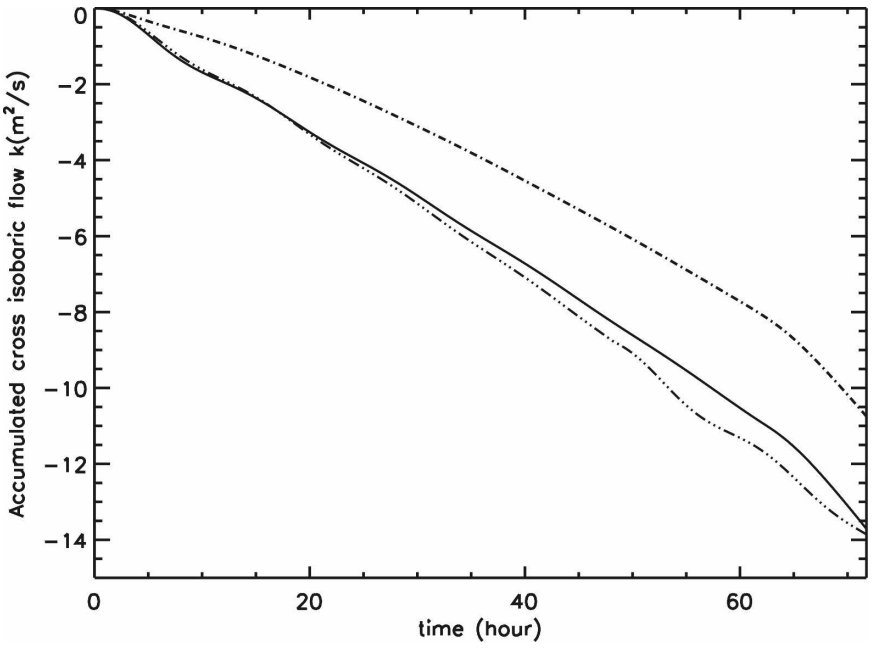

FIG. 7. Modeled accumulated cross-isobaric mass flow for using a short-tail formulation (dot–dashed line), a short-tail formulation plus wave stress according to Eq. (6) (solid line), and the LTGr formulation (dash–dot–dot–dotted line).

independent $\overline{v'w'}$ higher in the SBL corresponds to the modeled linear wind v profile and a nearly height-independent Ri in that layer.

After 8 h the turbulent stress $\overline{u'w'}$ equals the wave stress in the upper half of the SBL, and its magnitude is larger in comparison with the results from D91, and also near the surface the wave stress is substantial and dominant. The magnitude of the turbulent heat flux is slightly larger when compared with the D91 parameterization, but both are about a factor of 2 smaller than the LTGr formulation. Near the surface $\overline{u'w'}$ increases with height, caused by a reduced gradient of the near-surface wind speed profile.

d. Column model: Cyclone filling

As mentioned before, long tails (LTGr) play an obvious role in obtaining sufficient cyclone filling. Figure 7 shows cross-isobaric mass flow (as a measure of cyclone filling), calculated as $f\int_{z=0}^{z=z_{\mathrm{TOP}}} v(z)\,dz$ for a model integration of 68 h, for the short-tail formulation, for LTGr, and for the presented alternative with terrain stress. Surprisingly good correspondence is seen between cross-isobaric mass flow for the LTGr scheme and the current formulation that accounts for wave stress divergence. Thus, the incorporation of the wave stress divergence gives similar cross-isobaric mass flow, and at the same time a smaller (more realistic) boundary layer height, as well as a better representation of the LLJ.

Resolution dependence is an important issue for model parameterizations. We examined this sensitivity by rerunning the case study for 30 and 25 layers instead of 40, and at the same time increasing the height of the first model level. We found no major differences in the forecasted profiles and cross-isobaric flow.

An important advantage of the current proposal over the enhanced mixing approach is first that τ_{wave} vanishes in the case $N/U < k_s$ (i.e., where gravity waves cannot propagate), instead of being active for all stabilities. As such, the parameterization is more selective on physical grounds. Second, the scheme extracts mean momentum from the flow without extending the boundary layer too deeply, which will improve the forecast quality of minimum temperature, radiation fog, and surface frost.

5. Discussion

To further understand our findings, we consider the inclusion of wave drag on the stability function F_m [see Eq. (1)]. The appendix presents an apparent stability function (F_m^*) that includes wave drag, which reads

$$F_m^* = \frac{1}{\varphi_m^2} + \frac{k_s H^2 \sqrt{\mathrm{Ri}}}{2\kappa^2 z}. \tag{8}$$

The modified relationship includes an extra term to the original formulation from D91. This extra term is a

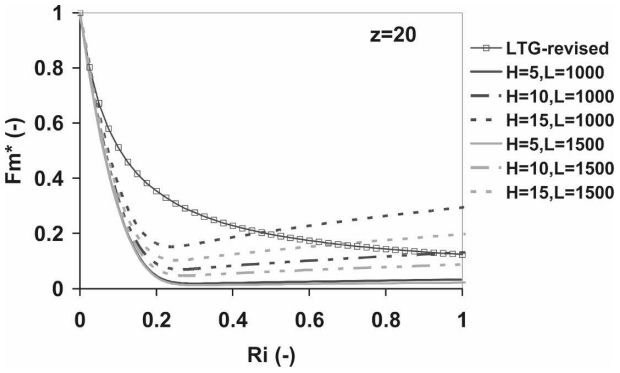

FIG. 8. Apparent stability function F_m^* as function of gradient Richardson number for orography with amplitude of 5, 10, and 15 m and wavelength of 1000 and 1500 m at 20-m height. The LTGr line corresponds to the current formulation in the ECMWF model.

function of Ri and indicates a stronger impact for stronger stability.

Figure 8 depicts Eq. (8) for small-scale orography ranging from $H = 5$ to 15 m and $L_x = 1000$ to 1500 m, together with the F_m formulation in the current ECMWF model (also known as LTGr; Beljaars and Viterbo 1998). The LTGr scheme allows more (but only turbulent) drag for large Ri while with Eq. (2) the turbulent drag nearly vanishes at Ri = 0.2. The LTGr scheme has a strong departure from D91's turbulence field observations for $0.1 < \text{Ri} < 0.2$.

Relative to the LTGr scheme, F_m^* has some characteristic advantages. First it satisfies Eq. (2) for $\text{Ri} < 0.2$ and is thus in closer agreement with field observations and LES for the weakly SBL (small Ri). At the same time, F_m^* approaches the long-tail formulation of LTGr for large Ri, but now physically based on the above considerations of terrain stress.

As a general comment, notice that using Ri as a stability measure in coarse-resolution models leads to overestimation of Ri, especially for strongly curved profiles. This might lead to erroneously turbulent mixing (Shir and Bornstein 1977; Walters et al. 2007). Our proposal [Eq. (7)] just circumvents using Ri.

We emphasize that Eq. (8) cannot be directly applied in practice in operational models. We present our results in this manner only because the enhanced mixing problem is often presented in this format. Since the physical mechanisms of turbulent mixing and wave stress are different, they should be treated separately in models (as in section 4). Note also that the parameterized wave drag does not include a companion transport of heat.

Our proposal is based on highly simplified physics of terrain stress in the SBL since we do not model the wave field itself, but only the net effect of gravity waves on the total drag on a large scale. The simplification lies in the fact that the linear theory is based on a sufficiently slow variation of the wind speed and stratification with height (i.e., the Wentzel–Kramers–Brillouin assumption). However, it is well known that the SBL is characterized by strong vertical gradients of wind speed and temperature (e.g., Balsey et al. 2003). Also, the majority of the theoretical work assumes a hyperbolic tangent wind speed profile in which a critical level is a priori present, although this is unrealistic for the major part of the SBL. In addition, large-scale models lack the ability to resolve this type of wind speed profile (and critical levels as well). Therefore, we have chosen to use this semiempirical and practical approach.

We would like to remark that SBL terrain stress is just one process that might be responsible for the missing drag. An alternative mechanism that could add drag over a longer time period could be due to nonlocal momentum mixing in the convective ABL (Frech and Mahrt 1995; Brown and Grant 1997; Beare 2007), which is typically not accounted for in most of the current-generation large-scale models. In the convective boundary layer, large eddies of the size of the whole ABL can transport momentum, scalars, and heat through the whole ABL. Current operational models (except for the Met Office model) only account for nonlocal transport of heat at best (e.g., Holtslag and Boville 1993).

Despite the potential impact of wave drag on small hills, direct field observations to validate the theory are currently missing. It would be desirable to have direct observations of wave drag for small hills, and therefore we recommend observations of wave drag (e.g., using microbarographs) for future experimental campaigns that focus on the SBL.

Considering earlier theoretical work on this subject, almost all previous studies of wave drag over orography used either monochromatic surface corrugation or idealized two- and three-dimensional obstacles. In these cases, the wave stress calculations are essentially two-dimensional (see, e.g., Kim and Mahrt 1992; Nappo and Chimonas 1992; Grisogono 1994; Dörnbrack and Nappo 1997; Nappo et al. 2004). Bretherton (1969), Hines (1988), and Shutts (1995) argued that the application of a two-dimensional wave stress parameterization to realistic three-dimensional subgrid-scale terrain is an oversimplification of the problem. Thus, it is inaccurate to replace three-dimensional terrain with monochromatic surface corrugations.

The results of such an approach are to overestimate the net wave stress. This is because a stably stratified flow over real topography will have wind components

passing over some obstacles. The magnitudes of these wind components are given by $u(\theta) = U\cos\theta$, where U is the surface wind speed and θ is the angle of the component. Because $u(\theta)$ decreases with increasing θ, the wave drag also decreases as $\theta \to \pi/2$. Accordingly, the average or net wave stress will be less than that estimated by assuming a uniform value of surface wind speed over all the terrain.

In the linear theory, each Fourier component of the surface terrain excites a wave response (Nappo 2002). Thus, the spectrum of gravity waves is a linear function of the spectrum of the terrain disturbances. In the three-dimensional case, a two-dimensional Fourier transform of the surface topography is required. Bretherton (1969), Young and Pielke (1983), and Bannon and Yuhas (1990) used the meridional average of the Fourier transform of the zonal components of the real two-dimensional terrain. However, such a method implies an isotropy of the topography as does the use of an effective surface roughness parameter (see, e.g., Mason 1988; Georgelin et al. 1994; Taylor et al. 1989). Shutts (1995) recognized the directionality of the two-dimensional Fourier transform of terrain-height variance. Accordingly, Shutts (1995) converted the two-dimensional Fourier transform of the surface terrain into polar coordinates, and evaluated the wave stress in this coordinate system.

In consideration of these remarks, we see that the results presented in this paper represent an upper bound of the wave stress. However, considering the uncertainty of applying linear theory to real, nonlinear flows, these estimates may not be unreasonably large. What is significant is the demonstration that the stress due to gravity waves in the SBL can be parameterized in a consistent and realistic way.

6. Conclusions

In this paper we analyze the possible role of subgrid terrain stress in the momentum budget of the stable boundary layer over land, relative to the role of turbulent drag. As a working hypothesis we assume that it is common practice for many numerical weather prediction models to need artificially more drag ("long tails") than is justified by turbulence in field observations. This is needed to obtain good skill scores on the synoptic flow. Theory shows that the sum of a simple estimate of the terrain drag and a realistic turbulent drag provides good correspondence with the drag obtained with the long-tail formulation. As such, the terrain stress may be a possible explanation for the need for long-tail mixing functions.

In addition, a simple and practical quasi-empirical parameterization of terrain drag divergence for use in large-scale models is proposed and is tested in a column mode. As an outcome, the cross-isobaric mass flow (a measure for cyclone filling) with the new scheme appears to be equal to what is found with the long-tail scheme. At the same time, the new scheme produces a much more realistic and less-deep boundary layer than using the long-tail mixing function. Finally, we recommend additional validation against observations, and in a full 3D forecast system.

Acknowledgments. We thank Arnold Moene (Wageningen University) for his comments on an earlier version of this manuscript.

APPENDIX

Derivation of an Apparent Stability Function

We introduce an apparent stability function F_m^*,

$$F_m^* = \frac{(\tau_{\text{turb}} + \tau_{\text{wave}})/\rho}{(\kappa z)^2\left(\frac{\partial U}{\partial z}\right)^2} = \frac{\tau_{\text{turb}}/\rho}{\left(\kappa z \frac{\partial U}{\partial z}\right)^2} + \frac{\tau_{\text{wave}}/\rho}{\left(\kappa z \frac{\partial U}{\partial z}\right)^2}, \tag{A1}$$

where τ_{turb} is the turbulent drag, τ_{wave} is the wave drag, ρ is air density, and z is the height above the surface. This results in (only for the lower part of the SBL: $H \ll z \ll h$, with h being the SBL depth)

$$F_m^* = \frac{u_*^2}{\left(\kappa z \frac{\partial U}{\partial z}\right)^2} + \frac{k_s H^2 UN}{2\left(\kappa z \frac{\partial U}{\partial z}\right)^2}. \tag{A2}$$

Recalling that $\varphi_m = (kz/u_*)(\partial U/\partial z)$, $S = \partial U/\partial z$, and $\text{Ri} = N^2/S^2$, and approximating $U = (\partial U/\partial z)z$, we obtain

$$F_m^* = \frac{1}{\varphi_m^2} + \frac{k_s H^2\sqrt{\text{Ri}}}{2\kappa^2 z}. \tag{A3}$$

We emphasize that Eq. (A3) cannot be directly applied in practice in operational models (see also the text). Note that formerly τ_{turb} and τ_{wave} cannot be a priori considered additive because wave stress will influence the wind speed and consequently this will alter the turbulence and vice versa. As a working hypothesis for this illustration, we assume the degree of interdependency is small and we assume both processes are additive.

REFERENCES

André, J. C., and L. Mahrt, 1982: The nocturnal surface inversion and influence of clear-air radiative cooling. *J. Atmos. Sci.,* **39,** 864–878.

Baas, P., G. J. Steeneveld, B. J. H. van de Wiel, and A. A. M.

Holtslag, 2006: Exploring self-correlation in flux gradient relationships for stably stratified conditions. *J. Atmos. Sci.,* **63,** 3045–3054.

Balsey, B., R. G. Frehlich, M. L. Jensen, Y. Meilleir, and A. Muschinski, 2003: Extreme gradients in the nocturnal boundary layer: Structure, evolution, and potential causes. *J. Atmos. Sci.,* **60,** 2496–2508.

Bannon, P. R., and J. A. Yuhas, 1990: On mountain wave drag over complex terrain. *Meteor. Atmos. Phys.,* **43,** 155–162.

Beare, R. J., 2007: Boundary layer mechanisms in extratropical cyclones. *Quart. J. Roy. Meteor. Soc.,* **133,** 503–515.

——, and Coauthors, 2006: An intercomparison of large-eddy simulations of the stable boundary layer. *Bound.-Layer Meteor.,* **118,** 247–272.

Belcher, S. E., and N. Wood, 1996: Form and wave drag due to stably stratified turbulent flow over low ridges. *Quart. J. Roy. Meteor. Soc.,* **122,** 863–902.

Beljaars, A. C. M., and A. A. M. Holtslag, 1991: Flux parameterization over land surfaces for atmospheric models. *J. Appl. Meteor.,* **30,** 327–341.

——, and P. Viterbo, 1998: Role of the boundary layer in a numerical weather prediction model. *Clear and Cloudy Boundary Layers,* A. A. M. Holtslag and P. G. Duynkerke, Eds., Royal Netherlands Academy of Arts and Sciences, 287–304.

——, A. R. Brown, and N. Wood, 2004: A new parameterization of turbulent orographic form drag. *Quart. J. Roy. Meteor. Soc.,* **130,** 1327–1347.

Bretherton, F. P., 1969: Waves and turbulence in stably stratified fluids. *Radio Sci.,* **4,** 1279–1287.

Brown, A. R., and A. L. M. Grant, 1997: Non-local mixing of momentum in the convective boundary layer. *Bound.-Layer Meteor.,* **84,** 1–22.

——, and N. Wood, 2001: Turbulent form drag on anisotropic three-dimensional orography. *Bound.-Layer Meteor.,* **101,** 229–241.

——, and ——, 2003: Properties and parameterization of the stable boundary layer over moderate topography. *J. Atmos. Sci.,* **60,** 2797–2808.

——, M. Athanassiadou, and N. Wood, 2003: Topographically induced waves within the stable boundary layer. *Quart. J. Roy. Meteor. Soc.,* **129,** 3357–3370.

——, A. C. M. Beljaars, H. Hersbach, A. Hollingsworth, M. Miller, and D. Vasiljevic, 2005: Wind turning across the marine atmospheric boundary layer. *Quart. J. Roy. Meteor. Soc.,* **131,** 1233–1250.

Businger, J. A., J. C. Wyngaard, Y. Izumi, and E. F. Bradley, 1971: Flux profile relationships in the atmospheric surface layer. *J. Atmos. Sci.,* **28,** 181–189.

Cheinet, S., A. Beljaars, M. Kohler, J.-J. Morcrette, and P. Viterbo, 2005: Assessing physical processes in the ECMWF model forecasts using the ARM SGP observations. ECMWF-ARM Report Series 1, 25 pp.

Cheng, Y., M. B. Parlange, and W. Brutsaert, 2005: Pathology of Monin-Obukhov similarity in the stable boundary layer. *J. Geophys. Res.,* **110,** D06101, doi:10.1029/2004JD004923.

Chimonas, G., and C. J. Nappo, 1989: Wave drag in the planetary boundary layer over complex terrain. *Bound.-Layer Meteor.,* **47,** 217–232.

Cuxart, J., and Coauthors, 2006: A single-column model intercomparison for a stably stratified atmospheric boundary layer. *Bound.-Layer Meteor.,* **118,** 273–303.

Dörnbrack, A., and C. J. Nappo, 1997: A note on the application of linear wave theory at a critical level. *Bound.-Layer Meteor.,* **82,** 399–416.

Duynkerke, P. G., 1991: Radiation fog: A comparison of model simulation with detailed observations. *Mon. Wea. Rev.,* **119,** 324–341.

Einaudi, F., and J. J. Finnigan, 1981: The interaction between an internal gravity waves and the planetary boundary layer. Part I: The linear analysis. *Quart. J. Roy. Meteor. Soc.,* **107,** 793–806.

Ek, M. B., K. E. Mitchell, Y. Lin, E. Rogers, P. Grunmann, V. Koren, G. Gayno, and J. D. Tarpley, 2003: Implementation of the Noah land surface model advances in the National Centers for Environmental Prediction operational mesoscale Eta model. *J. Geophys. Res.,* **108,** 8851, doi:10.1029/2002JD003296.

Eliassen, A., and E. Palm, 1960: On the transfer of energy in stationary mountain waves. *Geofys. Publ.,* **22,** 1–23.

Finnigan, J., 1999: A note on the wave-turbulence interaction and the possibility of scaling the very stable boundary layer. *Bound.-Layer Meteor.,* **90,** 529–539.

Frech, M., and L. Mahrt, 1995: A two-scale mixing formulation for the atmospheric boundary layer. *Bound.-Layer Meteor.,* **73,** 91–104.

Fritts, D. C., 1984: Shear excitation of atmospheric gravity waves. Part II: Nonlinear radiation from a free shear layer. *J. Atmos. Sci.,* **41,** 524–537.

Garratt, J. R., and R. A. Brost, 1981: Radiative cooling effects within and above the nocturnal boundary layer. *J. Atmos. Sci.,* **38,** 2730–2746.

Georgelin, M., E. Richard, M. Petitdidier, and A. Druilhet, 1994: Impact of subgrid-scale orography parameterization on the simulation of orographic flows. *Mon. Wea. Rev.,* **122,** 1509–1522.

Grant, A. L. M., 1994: Wind profiles in the stable boundary layer, and the effect of low relief. *Quart. J. Roy. Meteor. Soc.,* **120,** 27–46.

Grisogono, B., 1994: Dissipation of wave drag in the atmospheric boundary layer. *J. Atmos. Sci.,* **51,** 1237–1243.

Hines, C. O., 1988: A modeling of atmospheric gravity waves and wave drag generated by isotropic and anisotropic terrain. *J. Atmos. Sci.,* **45,** 309–322.

Holden, J. J., S. H. Derbyshire, and S. E. Belcher, 2000: Tethered balloon observations of the nocturnal stable boundary layer in a valley. *Bound.-Layer Meteor.,* **97,** 1–24.

Holtslag, A. A. M., 1998: Modeling of atmospheric boundary layers. *Clear and Cloudy Boundary Layers,* A. A. M. Holtslag and P. G. Duynkerke, Eds., Royal Netherlands Academy of Arts and Sciences, 85–110.

——, 2006: Special issue for boundary-layer meteorology: GEWEX Atmospheric Boundary-Layer Study (GABLS) on stable boundary layers. *Bound.-Layer Meteor.,* **118,** 241–243.

——, and B. A. Boville, 1993: Local versus nonlocal boundary layer diffusion in a global climate model. *J. Climate,* **6,** 1825–1842.

Howell, J. F., and J. Sun, 1999: Surface-layer fluxes in stable conditions. *Bound.-Layer Meteor.,* **90,** 495–520.

Jiang, Q., J. D. Doyle, and R. B. Smith, 2006: Interaction between trapped waves and boundary layers. *J. Atmos. Sci.,* **63,** 617–633.

Kim, J., and L. Mahrt, 1992: Momentum transport by gravity waves. *J. Atmos. Sci.,* **49,** 735–748.

Kurzeja, R. J., S. Berman, and A. H. Weber, 1991: A climatologi-

cal study of the nocturnal planetary boundary layer. *Bound.-Layer Meteor.,* **105,** 105–128.

Lott, F., and M. J. Miller, 1997: A new subgrid-scale orographic drag parameterization: Its formulation and testing. *Quart. J. Roy. Meteor. Soc.,* **123,** 101–127.

Louis, J. F., 1979: A parametric model of vertical eddy fluxes in the atmosphere. *Bound.-Layer Meteor.,* **17,** 187–202.

Mahrt, L., 1987: Grid-averaged surface fluxes. *Mon. Wea. Rev.,* **115,** 1550–1560.

Mason, P. J., 1988: The formation of areally-averaged roughness lengths. *Quart. J. Roy. Meteor. Soc.,* **114,** 399–420.

McCabe, A., and A. R. Brown, 2006: The role of surface heterogeneity in modelling the stable boundary layer. *Bound.-Layer Meteor.,* **122,** 517–534.

McVehil, G. E., 1964: Wind and temperature profiles near the ground in stable stratification. *Quart. J. Roy. Meteor. Soc.,* **90,** 136–146.

Nappo, C. J., 1991: Sporadic breakdowns of stability in the PBL over simple and complex terrain. *Bound.-Layer Meteor.,* **54,** 69–87.

——, 2002: *An Introduction to Atmospheric Gravity Waves.* Academic Press, 276 pp.

——, and G. Chimonas, 1992: Wave exchange between the ground surface and a boundary-layer critical level. *J. Atmos. Sci.,* **49,** 1075–1091.

——, H.-Y. Chun, and H.-J. Lee, 2004: A parameterization of wave stress in the planetary boundary layer for use in mesoscale models. *Atmos. Environ.,* **38,** 2665–2675.

Nielsen, N. W., and B. H. Sass, 2005: The effect of surface stress rotation on the Ekman pumping. HIRLAM Newsletter, Vol. 47, 1–8.

Oke, T. R., 1970: Turbulent transport near the ground in stable conditions. *J. Appl. Meteor.,* **9,** 778–786.

Palmer, T. N., G. J. Shutts, and R. Swinbank, 1986: Alleviation of a systematic westerly bias in general circulation and numerical weather prediction models through an orographic gravity wave drag parameterization. *Quart. J. Roy. Meteor. Soc.,* **112,** 1001–1039.

Poulos, G. S., and Coauthors, 2002: CASES-99: A comprehensive investigation of the stable nocturnal boundary layer. *Bull. Amer. Meteor. Soc.,* **83,** 555–581.

Rontu, L., 2006: A study on parameterization of orography-related momentum fluxes in a synoptic-scale NWP model. *Tellus,* **58A,** 69–81.

Shir, C. C., and R. D. Bornstein, 1977: Eddy exchange coefficients in numerical models of the planetary boundary layer. *Bound.-Layer Meteor.,* **11,** 171–185.

Shutts, G. J., 1995: Gravity-wave parameterization over complex terrain: The effect of critical-level absorption in directional wind-shear. *Quart. J. Roy. Meteor. Soc.,* **121,** 1005–1021.

Skibin, D., and J. A. Businger, 1985: The vertical extent of the log-linear wind profile under stable stratification. *Atmos. Environ.,* **19,** 27–30.

Steeneveld, G. J., B. J. H. van de Wiel, and A. A. M. Holtslag, 2006a: Modeling the evolution of the atmospheric boundary layer coupled to the land surface for three contrasting nights in CASES-99. *J. Atmos. Sci.,* **63,** 920–935.

——, ——, and ——, 2006b: Modelling the Arctic stable boundary layer and its coupling to the surface. *Bound.-Layer Meteor.,* **118,** 357–378.

——, ——, and ——, 2007: Diagnostic equations for the stable boundary layer height: Evaluation and dimensional analysis. *J. Appl. Meteor. Climatol.,* **46,** 212–225.

——, T. Mauritsen, E. I. F. de Bruijn, J. Vilá-Guerau de Arellano, G. Svensson, and A. A. M. Holtslag, 2008: Evaluation of limited-area models for the representation of the diurnal cycle and contrasting nights in CASES-99. *J. Appl. Meteor. Climatol.,* **47,** 869–887.

Sun, J., and Coauthors, 2003: Atmospheric disturbances that generate intermittent turbulence in nocturnal boundary layers. *Bound.-Layer Meteor.,* **110,** 255–279.

Taylor, P. A., R. I. Sykes, and P. J. Mason, 1989: On the parameterization of drag over small-scale topography in neutrally-stratified boundary-layer flow. *Bound.-Layer Meteor.,* **48,** 409–422.

Vickers, D., and L. Mahrt, 2004: Evaluating formulations of the stable boundary layer height. *J. Appl. Meteor.,* **43,** 1736–1749.

Viterbo, P., A. Beljaars, J. F. Mahfouf, and J. Teixeira, 1999: The representation of soil moisture freezing and its impact on the stable boundary layer. *Quart. J. Roy. Meteor. Soc.,* **125,** 2401–2426.

Walters, J. T., R. T. McNider, X. Shi, W. B. Norris, and J. R. Christy, 2007: Positive surface temperature feedback in the stable nocturnal boundary layer. *Geophys. Res. Lett.,* **34,** L12709, doi:10.1029/2007GL029505.

Wood, N., and P. J. Mason, 1993: The pressure force induced by neutral, turbulent flow over hills. *Quart. J. Roy. Meteor. Soc.,* **119,** 1233–1267.

Young, G. S., and R. A. Pielke, 1983: Application of terrain height variance spectra to mesoscale modeling. *J. Atmos. Sci.,* **40,** 2555–2560.

Zilitinkevich, S. S., 2002: Third-order transport due to internal waves and non-local turbulence in the stably stratified surface layer. *Quart. J. Roy. Meteor. Soc.,* **128,** 913–925.

——, V. L. Perov, and J. C. King, 2002: Near-surface turbulent fluxes in stable stratification: Calculation techniques for use in general circulation models. *Quart. J. Roy. Meteor. Soc.,* **128,** 1571–1587.